Original Research Article

DFT Study of Bismide Ternary Alloys $GaAs_{1-x}Bi_x$: Structural, Electronic, and Optical Properties

Akeem.A Adewale[1,2,6], C.De Conti[2], Surajudeen Otolowo Azeez[1,3*], kamaldeen.O Suleman[4], Hakeem O. Oyeshola[1], Ayodele Joshua Abiodun[5], Lukmam Ayobami Sunmonu[1]

[1]*Department of Pure and Applied Physics, Ladoke Akintola University of Technology, Ogbomoso, Nigeria*
[2]*School of Engineering and Sciences, São Paulo State University (UNESP), Rosana, SP 19274-000, Brazil*
[3]*Department of Physical and Chemical Sciences, Federal University of Health Sciences, Ila- Orangun, Nigeria*
[4]*Department of Physics, Nigeria Maritime University, Okerenkoko, Warri, Nigeria*
[5]*Department of Physics, Lead City University, Ibadan, Nigeria*
[6]*Nanotechnology Research Group (NANO+), Ladoke Akintola University of Technology, Ogbomoso, Nigeria*

Citation A.A. Adewale, C. De Conti, S. O. Azeez, K.O. Suleman, H.O. Oyeshola, A.J. Abiodun , L.A. Sunmonu. DFT Study of Bismide Ternary Alloys $GaAs_{1-x}Bi_x$: Structural, Electronic, and Optical Properties. *J. Eng. Ind. Res.* **2025**, 6(4):337-351.

https://doi.org/10.48309/jeires.2025.530888.1245

CC BY

Article info:
Submitted: 2025-06-20
Revised: 2025-07-18
Accepted: 2025-08-11
ID: JEIRES- 2506-1245

Keywords:
Alloy; Dopant; Electronic structure; Modeling; Optical properties.

ABSTRACT

Gallium Arsenide Bismide (GaAsBi) is a III-V semiconductor alloy formed by adding bismuth (Bi) to gallium arsenide (GaAs), resulting in a reduced bandgap and improved optoelectronic properties. Its unique characteristics make it a promising material for advanced photodetector applications and high-efficiency solar cells. The structural, electronic, and optical properties of pristine Gallium Arsenide (GaAs) and its alloy $GaAs_{1-x}Bi_x$ (x = 0.25, 0.5, 0.75, 1) compounds were explored using the first principle approach with a full potential linear augmented plane wave (FPLAPW) method as implemented in WIEN2K code. The structural properties, including lattice constant, volume, and bulk modulus, were assessed after optimization using Murnaghan's equation of state. Electronic properties were determined using two methods such as the generalized gradient approximation in Perdew-Burke-Ernzerhof (PBE) and the modified Becke-Johnson (mBJ) approach for the exchange-correlation potential. Optical parameters including absorption coefficient, reflectivity, conductivity, and others were simulated from a computed dielectric function using the Kramers-Kronig relation.

Surajudeen O. Azeez (surajudeen.azeez@fuhsi.edu.ng)

Introduction

The group III-V semiconductors and their alloys have received considerable interest due to their widespread utility in thermoelectric, spintronic, thermodynamic, and optical sensor applications [1-4]. The most prominent III-V semiconductor is GaAs. It was established that doping on GaAs with Bi affects the spectroscopic characteristics and electronic properties. Likewise, the forbidden energy range exhibits a modification as the Bi replaces As due to variations in the atomic radii of the two atoms [5]. This variation can lead to different features. Firstly, there will be a band gap reduction as the impurity is present. Additionally, the spin-orbit interaction prompts the energy bands to split. This causes asymmetrical energies corresponding to electron spin orientations. Meanwhile, the presence of Bi induces the stability of their thermodynamic alloys. High levels of dopants of Bi reduce GaAs stability.

Currently, the research on the energy band gap of GaAsBi has been widely investigated. The thermoelectric properties of bismuth-based $GaAs_{1-x}Bi_x$ semiconductors for improved energy conversion efficiency were examined [6]. It was found that substituting As atoms with Bi atoms (GaBi) caused a less reduction of electronic thermal conductivity compared to that of GaAs. Likewise, the thermal conductivity exhibits a downward trend with increasing x due to the heavy atom nature of bismuth leading to enhanced phonon scattering, which affects its thermal properties [6]. STEM techniques were used to analyze the distribution of Bi in $GaAs_{1-x}Bi_x$ epilayers fabricated using molecular beam epitaxy [7]. Atomic-resolution energy-dispersive X-ray spectroscopy (EDX) combined with high-angle annular dark-field (HAADF) imaging revealed that the characteristic CuPt-type ordering is modulated periodically along the [001] direction, with varying Bi distributions within the alloy [7]. The energy band gap calculation of $GaAs_{1-x}Bi_x$ with 12% bismuth using a tight-binding approach, reveals that the forbidden energy gap narrowing is a consequence of an increase due to varied Bi-As interactions [8]. Additionally, the energy band gap in dilute bismuth alloys based on the LDA functional approach confirms that bismuth states are observed below the valence band edge of GaAs upon partial substitution of As atoms with Bi [9]. In a study of energy band gap of $GaBi_xAs_{1-x}$ with the As-rich range was calculated using the first-principle method as well as the modified band anti-crossing (BAC) model [6]. It was found that the presence of Bi in GaAs changes material from a semiconductor to a metallic nature. The atomic size disparity leads to a stronger correlation between the Bi-level and the Γ VBM in GaAs than in GaSb. It was also noted that electronegativity variances between Bi and As atoms in GaAsBi are greater than Bi and Sb atoms in GaSbBi.

Nevertheless, III–V alloys persist in investigation, stressing the necessity for computational inquiries to elucidate additional properties such as; optical, electronic, and others. Most computational studies have focused on GaAsBi [7-9], noting a significant effect of Bi on electronic properties, especially energy band gap narrowing. This research aims to fill gaps in GaAsBi studies by employing WIEN2k software [10] with the Perdew-Burke-Ernzerhof functional in the Generalized Gradient Approximation (GGA-PBE) framework, based on Hohenberg-Kohn-Sham theory (DFT) [11]. The electronic band gap was initially computed using the standard DFT technique. Subsequently, the calculation was then refined by employing the Tran-Blaha modified Becke-Johnson (TB-mBJ) functional [12] to rectify the inherent underestimation of band gaps typically associated with standard DFT. We observed a significant gap in research on GaAsBi alloys, particularly regarding their optical properties. This lack of comprehensive exploration motivated our study, aiming to expand the understanding of both the optical and electronic characteristics of bismuth incorporation in GaAs. Through this work, we aim to contribute valuable insights that can advance the development of GaAsBi-based materials for

optoelectronic applications. Furthermore, the optical properties, including electrical conductivity, energy dissipation, absorption coefficient, optical refractive index, and reflectance, can be inferred from the dielectric response function. The electronic properties of GaAs and its Bi-alloyed counterparts were investigated by calculating their electronic band structures and the density of states. The $GaAs_{1-x}Bi_x$ alloys are attractive candidates for optoelectronic applications, as incorporating high atomic mass bismuth atoms is expected to reduce thermal conductivity through enhanced phonon interactions.

Computational details

This study investigates the geometrical, electronic, and optical properties of GaAs and its $GaAs_{1-x}Bi_x$ alloy compounds (x = 0, 0.25, 0.5, 0.75, 1) by employing DFT calculations implemented in the WIEN2K software within the full-potential linearized augmented plane wave (FP-LAPW) framework [10]. We executed the DFT, PBE-GGA exchange-correlation potential. The TB-mBJ method was applied to rectify the accuracy of band gap energies caused by the functionals. This approach approximates the atomic exact-exchange potential locally and incorporates a screening term. The spherical harmonic wave contributions were set to l_{max} = 10 for non-overlapping muffin-tin spheres, and at G_{max} = 12 $a.u.^{-1}$ the Fourier transform of the charge density develops. In the plane wave expansion, the cutoff parameter is K_{max} = 8/Rmt. A k-point value of 1000 was used in the complex wedge of the irreducible Brillouin zone (IBZ) in the self-consistent field (SCF) calculation.

The density of states (DOS) is simulated using the tetrahedral interpolation techniques [13], which utilize energy eigenvalues and eigenvectors at specific k-points. The electronic band structures were computed at high-symmetry k-vectors within the Brillouin zone using the exact diagonalization method. Monkhorst-Pack system [14] k-points of a highly dense mesh of 17×17× 17 and 21×21× 21 were set for DOS and optical parameter calculations, respectively, since they required better results.

Furthermore, optical spectra were evaluated from the complex dielectric function; real $\varepsilon_1(\omega)$ and imaginary $\varepsilon_2(\omega)$ parts (ω), depend on incident electromagnetic waves. From the dispersion relation [15], $\varepsilon_2(\omega)$ can be computed, and on it, other optical parameters are formulated.

Results and Discussion

Geometry optimization

The $GaAs_{1-x}Bi_x$ compounds (x = 0, 0.25, 0.5, 0.75, 1) structural analysis is investigated in this section. A cubic crystal system with a space group of F-43 m (No. 216) was adopted for GaAs [16]. In Figure 1, the VESTA software presents the physical structure of GaAs and its modeled alloys [17]. Here, Ga is a cation, and As is an anion. The Ga atom is located at Wyckoff coordinates of (0, 0, 0), while the As atom occupies the position (1/4, 1/4, 1/4). The crystal structure of GaAs is zinc-blende (face-centered cubic), with a lattice constant of 5.653 Å [18].

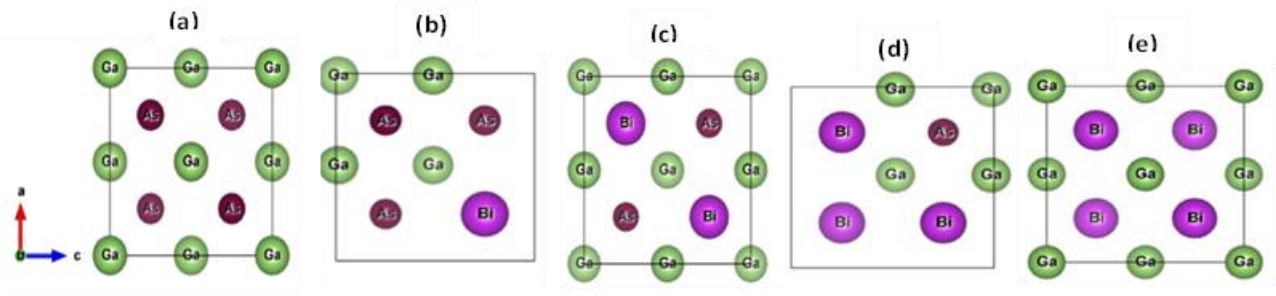

Figure 1(a-e): Crystal structure of $GaAs_{1-x}Bi_x$ compounds (x = 0, 0.25, 0.5, 0.75, 1).

The samples were optimized using Murnaghan's equation of state [19]. The energy-volume analysis for all the samples is illustrated in Figure 2, where the volume increases, the

energy decreases ultimately reaching a minimum value. The minimum energy value represents the ground state energy. The calculated ground state energy and equilibrium volume serve as the basis for determining the optimal structural parameters.

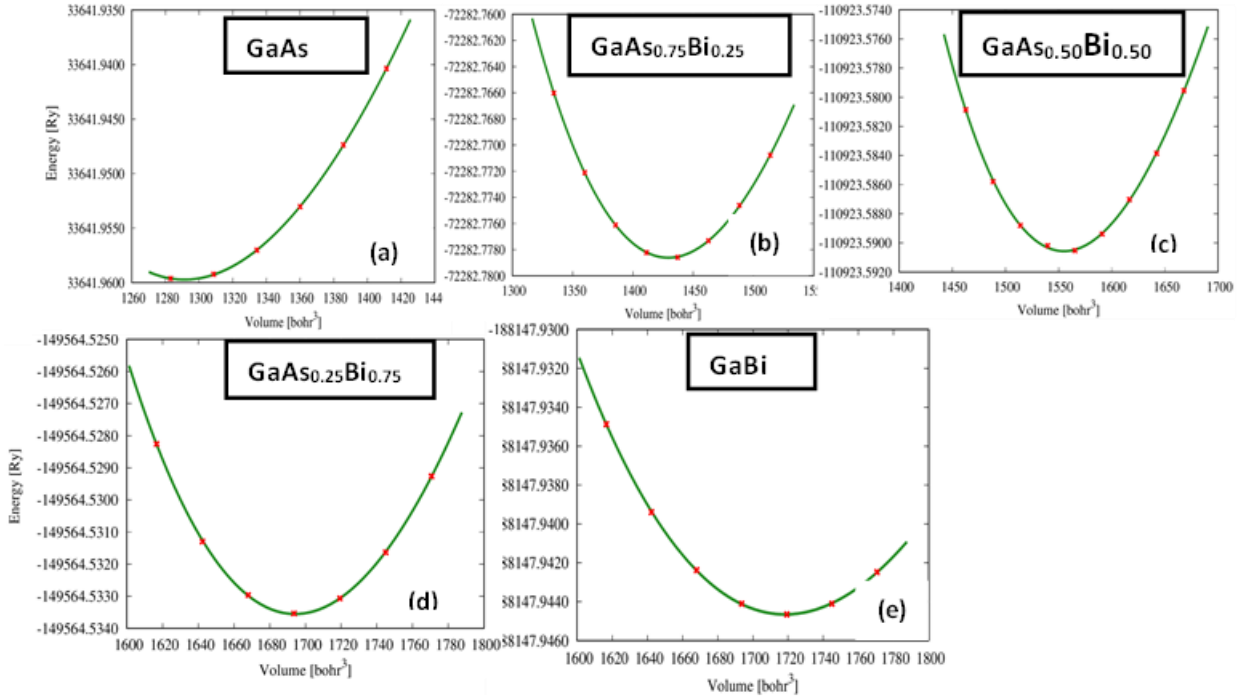

Figure 2(a-e): Total energy per atom as a function of volume for $GaAs_{1-x}Bi_x$ compounds (x = 0, 0.25, 0.5, 0.75, 1).

Our computed lattice constant, bulk modulus, and derivative of bulk modulus are presented in Table 1. These are closely correlated with several theoretical [20-29] and experimental works [30-32]. The substitution of As with larger atoms, such as Bi, generally results in an increased lattice parameter. However, this substitution also leads to a weakening of interatomic forces, causing a decrease in bulk modulus. This phenomenon accounts for the observed inverse correlation between lattice parameter and bulk modulus.

Table 1: Effect of composition (x) on lattice parameters(a), the bulk modulus (B), and derivatives of the bulk modulus (B′) in $GaAs_{1-x}Bi_x$ compounds

Compound	Parameter	Present work	Other theoretical	Experimental
GaAs	a(Å)	5.750	5.75 [20], 5.67 [21], 5.76 [22], 5.65 [23], and 5.62 [24]	5.65 [30] and5.64 [31]
	B(GPa)	58.357	61.78 [20], 71.78 [24], and 60.90 [25]	77.00 [31]
	B′	3.593	4.31[20] and 4.64 [24]	
$GaAs_{0.75}Bi_{0.25}$	a(Å)	5.972	6.20 [20], 6.04 [22], and 5.81[24]	
	B(GPa)	51.450	37.76 [20] and 62.22 [24]	
	B′	4.625	4.71 [20], 4.04 [24]	
$GaAs_{0.50}Bi_{0.50}$	a(Å)	6.144	6.36 [20] and 5.81[24]	

	B(GPa)	45.514	34.15 [20] and 53.98 [24]	
	B′	5.223	3.75 [20] and 4.63 [24]	
$GaAs_{0.25}Bi_{0.75}$	a(Å)	6.308	6.44 [20] and 6.33 [22]	
	B(GPa)	39.838	31.15 [20] and 43.25[24]	
	B′	4.843	5.00 [20] and 4.84 [24]	
GaBi	a(Å)	6.339	6.52 [20], 6.45 [26], 6.32 [23], 6.30 [27], and 6.23 [28]	6.32 [30,32]
	B(GPa)	42.393	31.06 [20], 41.06 [28], 45.1 [29], 46.37 [28]	
	B′	4.702	4.20 [20], 4.37 [26], 4.90 [29], and 4.35 [28]	

Electronic properties

To investigate the electronic properties of $GaAs_{1-x}Bi_x$ alloys, we performed; band structure, partial density of states (PDOS), and total density of states (TDOS) calculations. The electronic properties of III-V-Bi bismides differ from those of the other elements in group V due to the large size and low electronegativity of Bi. We studied the electronic properties of $GaAs_{1-x}Bi_x$ compounds in zinc-blende structure using PBE-GGA and TB-mBJ methods.

Electronic band structure

Figure 3 shows the band gap as a function of Bi dopant, calculated by two exchange-correlation models. PBE-GGA predicts metallic behavior, except in GaAs, which reveals semiconductor features as summarized in Table 2 and Figure 3. The electronic band structures of $GaAs_{1-x}Bi_x$ alloys calculated by TB-mBJ are shown in Figure 4(a-e). Note that the valence band maximum (VBM) and conduction band minimum (CBM) are at Γ point, indicating a direct band gap. The band gap energies for different Bi dopants (x) are presented in Table 2.

Table 2: Calculated band gap of $GaAs_{1-x}Bi_x$ compounds (x = 0, 0.25, 0.5, 0.75, 1)

Samples	Present work		Other theoretical work	Experimental
	GGA-PBE	TB-mBJ		
GaAs	0.6962	1.5971	1.41[8], 1.2 [20], 1.52 [22], and 1.51 [32]	1.52 [30]
$GaAs_{0.75}Bi_{0.25}$	0.0642	0.6524	0.449 [8], 0.38 [20], and 0.43 [22]	
$GaAs_{0.50}Bi_{0.50}$	0.000	0.2942	0.052 [8]	
$GaAs_{0.25}Bi_{0.75}$	0.000	0.2413	0.016 [8]	
GaBi	0.000	0.0362	-0.0056 [8], 1.45 [22], and -1.38 [20]	0.036 [33]

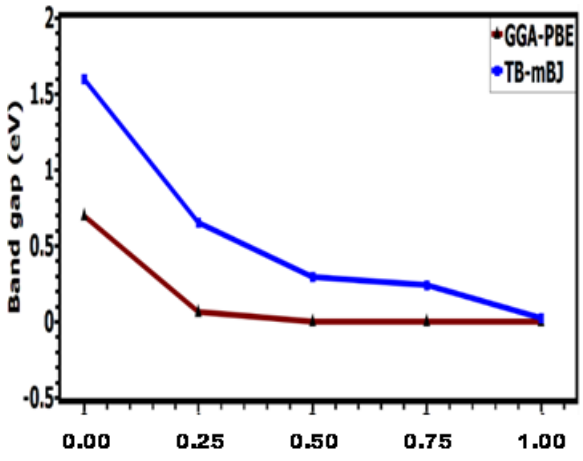

Figure 3: Variation in band gap as dopant rate x increased for $GaAs_{1-x}Bi_x$ compounds (x = 0, 0.25, 0.5, 0.75, 1).

The calculated band gap values are in good agreement with experimental data [30,32], which show the strong band gap bowing with increasing Bi dopant levels. This agreement confirms the accuracy of TB-mBJ exchange-correlation potentials. The decrease of band gap with increasing Bi is due to the atomic scale disruption induced by Bi dopant [8,33]. The main mechanism is structural relaxation and charge exchange, caused by the differences in atomic orbital size and energy between As and Bi atoms. The large decrease in the band gap can be also explained by the resonant interaction between the 6p orbital of Bi in the conduction band and valence band maximum (VBM) [8].

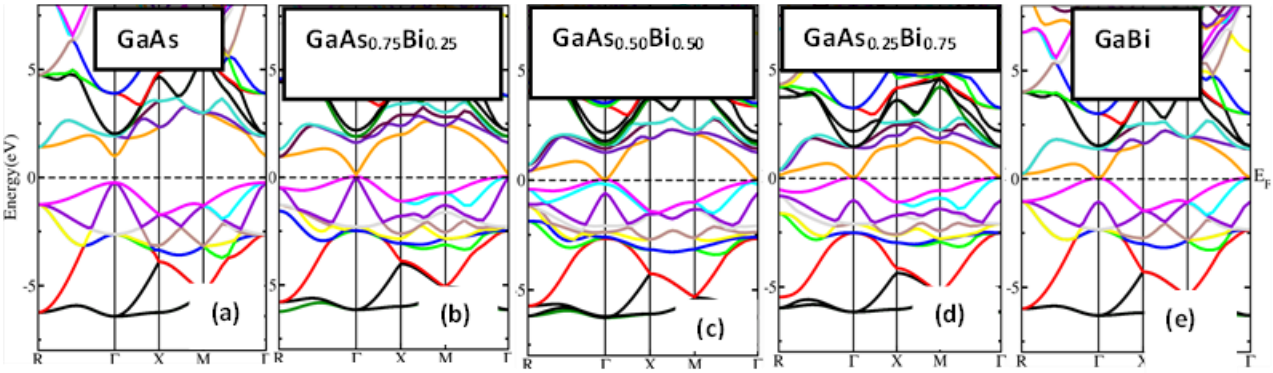

Figure 4(a-e): Calculated band structure for $GaAs_{1-x}Bi_x$ compounds (x = 0, 0.25, 0.5, 0.75, 1).

Density of state

The density of state (DOS) is an important concept for understanding the electronic behavior of materials, especially the electron transitions between different energy levels. Along with the band structure, DOS provides us valuable information on the electron movement between conduction and valence bands. Moreover, DOS controls the electron transitions between energy levels. Introducing dopants can significantly change the DOS of a material and its electronic properties, including optical parameters [26,36]. Figures 5(a-e) display the

computed density of states (TDOS and PDOS) for $GaAs_{1-x}Bi_x$ compounds (x = 0, 0.25, 0.5, 0.75, 1) using TB-mBJ methods. The TDOS for spin-up and spin-down states is presented. The Fermi energy is set to zero. The band gap is the energy region between VBM and CBM. The conduction band lies to the right of the Fermi level, while the valence band is on the opposite side.

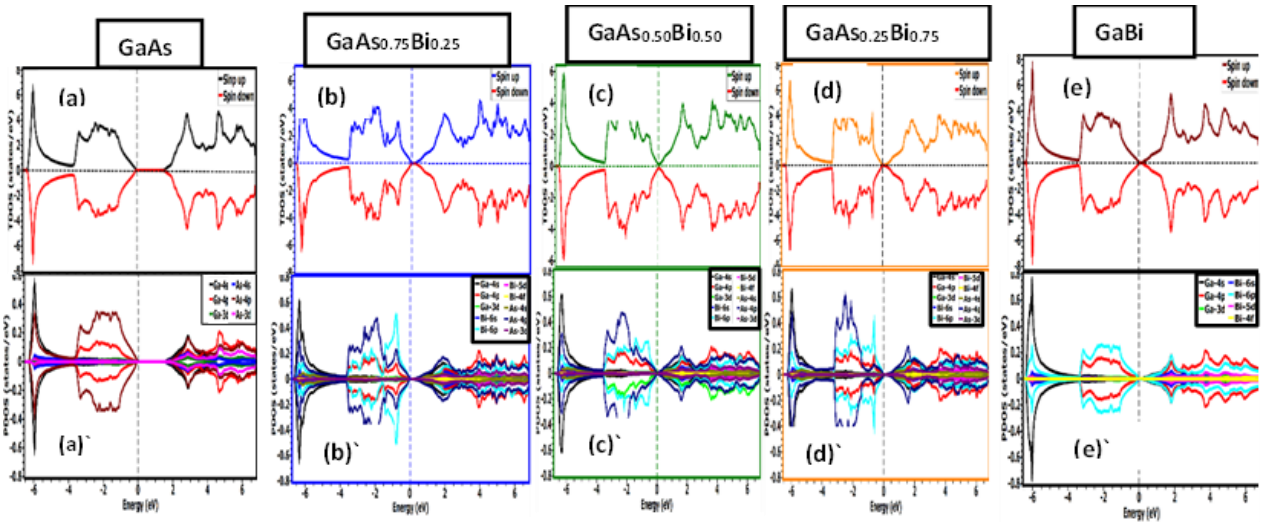

Figure 5(a-e): Total and Partial density of state for $GaAs_{1-x}Bi_x$ compounds (x = 0, 0.25, 0.5, 0.75, 1).

Figure 5(a-e) presents the PDOS of the studied compounds. In this case, the particular orbital contributing to each region is revealed. The As-4p orbital contribution is majorly at the conduction band near the Fermi level followed by Ga-4p. The Ga-4s states, dominate other orbitals such as As-4p, Ga-4p, As-4s, and others at the valence band. Our results are in good agreement with related work [20]. In the presence of Bi dopant, it was observed that Bi-6p dominates the conduction band region near the Fermi level in all model compounds ($GaAs_{1-x}Bi_x$ (x = 0.25, 0.5, 0.75, 1). This phenomenon likely results in a reduced band gap, accompanied by an expansion of the lattice constant, as observed in the structural analysis. Meanwhile, As-4p still dominates the valence band of the model samples.

Optical properties

In calculations of optical properties, a standard approach is to calculate the complex dielectric function, which serves as a fundamental quantity for deriving other optical parameters. Figure 6(a-h) presents the computed optical parameters for an incident photon energy range of 0-27 eV.

Dielectric function

The complex dielectric constant ε is given as follows [37]:

$$\varepsilon(\omega) = \varepsilon_1(\omega) + i\varepsilon_2(\omega) \quad (1)$$

Here, $\varepsilon(\omega)$ represents the complex dielectric function, where $\varepsilon_1(\omega)$ and $\varepsilon_2(\omega)$ correspond to its real and imaginary components, respectively. From the Kramers-Kronig transformation, the $\varepsilon_2(\omega)$ can be expressed as Equation (3) [38].

$$\varepsilon_2(\omega) = \frac{Ve^2}{2\pi\hbar m^2\omega^2}\int d^3k \sum_{m'} \left|\langle \vec{k}n|P|\vec{k}n'\rangle\right|^2 f_n^{\vec{k}}\left(1 - f_n^{\vec{k}'}\right)\delta\left(E_{n'}^{\vec{k}} - E_{n'}^{\vec{k}} - \hbar\omega\right) \quad (2)$$

Here, $\omega, e, k, and\ P$ represent the electromagnetic angular frequency, electron charge, wave vector, and momentum operator, respectively, while n and n' denote the initial and final electronic states, with $f_n^{\vec{k}}$ and $\delta\left(E_{n'}^{\vec{k}} - E_{n'}^{\vec{k}} - \hbar\omega\right)$ representing the Fermi distribution and Dirac delta functions. The $\varepsilon_2(\omega)$ serves as a quantitative indicator of a material's absorption properties and can be theoretically evaluated using electronic structure calculations [39].

The real part, $\varepsilon_1(\omega)$, is intrinsically linked to the imaginary part via the Kramers-Kronig relation [37].

$$\varepsilon_1(\omega) = 1 + \frac{2}{\pi} A \int_0^{\infty} \frac{\omega' \varepsilon_2(\omega')}{\omega'^2 - \omega^2} d\omega' \quad (3)$$

The expression for $\varepsilon_1(\omega)$ characterizes the material's electric polarizability and absorption behavior, offering valuable insight into its optical response as presented in Equation (3). Figure 6(a-b) illustrates the calculated dielectric function (ε) of GaAs1-xBix compounds (x = 0, 0.25, 0.5, 0.75, 1). The real part of the dielectric function exhibits a positive value within the 0 to ~3.17 eV photon energy range (visible region), followed by a transition to negative values above -3.2 eV (ultraviolet region). These suggest the presence of plasmon excitations in this energy regime, as shown in Figure 6(a). The highest static real dielectric constant was observed in $GaAs_{0.50}Bi_{0.50}$ (90.8), followed by $GaAs_{0.25}Bi_{0.75}$ (38.7), GaBi (29.7), $GaAs_{0.75}Bi_{0.25}$ (25.3), with the lowest value of 15.1 recorded for GaAs. For the imaginary part of the dielectric constant shown in Figure 6b, $GaAs_{0.5}Bi_{0.5}$ exhibits the highest value of 31.7 at 2.2 eV in the visible region. However, the peak values of the other materials occur in the ultraviolet region: GaAs (27.4 at 4.12 eV), $GaAs_{0.75}Bi_{0.25}$ (18.6 at 3.9 eV), $GaAs_{0.25}Bi_{0.75}$ (18.1 at 3.3 eV), and GaBi (25.1 at 3.3 eV). The observed peaks in the imaginary part of the dielectric constant, indicate strong absorption at specific photon energies. These peaks correspond to interband transitions, where electrons are excited from the valence band to the conduction band [40]. The position of these peaks reflects the energy required for such electronic transitions, with higher peak energies indicating transitions occurring in the ultraviolet region. Therefore, materials exhibiting peaks at higher energies absorb strongly in the UV spectrum. At lower photon energies, both the real and imaginary components of the dielectric function attain high values, gradually diminishing as the photon energy increases.

Absorption coefficient

The absorption coefficient quantifies the extent to which light is absorbed per unit length in optoelectronic materials [41]. Significant absorption occurs when the photon's energy surpasses the material's bandgap, facilitating electron transitions from the valence band to the conduction band [42]. This process is fundamental in devices such as photodetectors and solar cells, where efficient light absorption is crucial for optimal performance. The absorption coefficient was calculated using Equation (4) [32]:

$$\alpha(\omega) = \frac{\sqrt{2}\omega}{c} \sqrt{\sqrt{{\varepsilon_1}^2(\omega) + {\varepsilon_2}^2(\omega)} - \varepsilon_1(\omega)} \quad (4)$$

Where, c is the velocity of light.

The energy-dependent absorption coefficient of GaAs1-xBix compounds (x = 0, 0.25, 0.5, 0.75, 1) is depicted in Figure 6(c). The absorption coefficient exhibits a notable increase with rising energy, signifying an enhanced probability of electronic transitions from the valence band to the conduction band, particularly in the visible region. This is generally observed across all studied samples. Meanwhile, a prominent absorption peak in the ultraviolet (UV) region was observed in the absorption spectra, indicating a strong affinity for light absorption at this spectral range [43]. Thus, it may be used as a UV-detector and solar cell window material [32]. A distinct absorption peak was observed above the UV energy region in $GaAs_{0.5}Bi_{0.5}$, corresponding to the Bi atomic absorption edge, suggesting the presence of bismuth in the compound and offering insights into its local electronic and geometric configuration.

Refractive index

The refractive index characterizes how light travels through a specific material, describing the speed and direction of light propagation within it. The refractive index, which varies with energy, was determined by Equation (5) [25].

$$n(\omega) = \left[\frac{1}{2}\left(\varepsilon_1{}^2(\omega) + \varepsilon_2{}^2(\omega)\right)^{\frac{1}{2}} + \varepsilon_1(\omega)\right]^{1/2} \quad (5)$$

In the low-frequency limit (ω = 0), $n(0) = \sqrt{\varepsilon_1(0)}$, the equation reduces to one that corresponds to the material's static refractive index and static dielectric constant, describing its optical and electrical properties at zero frequency.

Additionally, the refractive index was further analyzed using well-established models, including those by Ravindra and Hervé-Vandamme [25], which relate the refractive index to the fundamental energy bandgap. These models are outlined below:

Ravindra model is expressed in Equation (6).

$$n(0) = M + \beta \cdot E_g \quad (6)$$

Where, $M = 4.084$ and $\beta = 0.62\ eV^{-1}$.

Hervé-Vandamme model is expressed in Equation (7).

$$n(0) = \left[1 + \left(\frac{A}{E_g + \beta}\right)\right]^{\frac{1}{2}} \quad (7)$$

Where, A= 13.6 and $\beta = 3.4\ eV$.

In Table 3, the static refractive indices of $GaAs_{1-x}Bi_x$ compounds (x = 0, 0.25, 0.5, 0.75, 1) are presented. Likewise, the static refractive index is associated with low absorption energy. It was also observed that as absorption increased, the corresponding refractive index decreased accordingly. Figure 6(d) depicts the behavior of the refractive index coefficient, as a function of energy. It is important to acknowledge that the refractive index experiences a significant decrease as an increase in the photon energy range within the visible region for all studied compounds. GaAs and GaBi exhibit a prominent peak in the refractive index, reaching 41.3 at 4.0 eV and 28.5 at 3.20 eV, respectively. This makes them highly suitable for integration into photonic systems [44]. Thus, these studied materials are generally highly significant for optoelectronic applications due to their refractive indices, which fall within the infrared spectrum range of 2.29-2.77 [16].

Table 3: The static refractive indices of $GaAs_{1-x}Bi_x$ compounds (x = 0, 0.25, 0.5, 0.75, 1)

Compounds	TB-mBJ	Ravindra model	Hervé-Vandamme model
GaAs	3.88	5.07	2.90
$GaAs_{0.75}Bi_{0.25}$	5.08	4.49	3.50
$GaAs_{0.50}Bi_{0.50}$	9.74	4.27	3.81
$GaAs_{0.25}Bi_{0.75}$	6.28	4.23	3.87
GaBi	5.48 and 4.65 [26]	4.11 and 4.08[26]	4.08 and 4.12 [26]

Optical conductivity

Optical conductivity (σ) is a fundamental parameter that characterizes a material's response to incident electromagnetic radiation [45]. The optical conductivity was calculated using the expression in Equation (8).

$$\sigma(\omega) = -i\frac{\omega}{4\pi}|\varepsilon(\omega) - 1| \quad (8)$$

It connected with the absorption coefficient and refractive index through the relation in Equation (9).

$$\sigma(\omega) = \frac{\alpha(\omega)n(\omega)}{4\pi} \quad (9)$$

When a material absorbs energy from incident photons, electrons are excited to higher energy states, creating free charge carriers. This phenomenon is quantified by the material's optical conductivity, which describes the relationship between the induced current density and the applied electric field across various frequencies. In this study, the optical conductivity spectra of the examined samples are depicted in Figure 6(e). The data reveal a

pronounced peak in the ultraviolet region, aligning with previous findings on the high absorptivity of these materials in this spectral range. It demonstrates the generation of free carrier due to incident absorption energy. Hence, the generation of free electrons induces a net forward current. We observed that the oscillations in optical conductivity beyond the ultraviolet energy range exhibit a similar trend to the variations in the refractive index, corroborating the relationship described in Equation (6). Interestingly, all the examined compounds displayed a sharp peak in optical conductivity in the UV region. Notably, GaAs displayed a prominent peak, suggesting high carrier mobility and efficient charge carrier conduction, surpassing the other compounds in this regard. Furthermore, the peaks in optical conductivity observed in the ultraviolet range are likely attributed to interband electronic transitions [46].

Extinction coefficient

The extinction coefficient (k) quantifies a material's ability to absorb light. It is a dimensionless parameter that represents the reduction in light intensity as it travels through the material. We calculate the extinction coefficient using Equation (10).

$$k(\omega) = \left[\frac{\sqrt{{\varepsilon_1}^2(\omega) + {\varepsilon_2}^2(\omega)} - \varepsilon_1(\omega)}{2}\right]^{1/2} \quad (10)$$

The calculated extinction coefficients of $GaAs_{1-x}Bi_x$ compounds (x = 0, 0.25, 0.5, 0.75, 1) were plotted in Figure 6(f). The extinction coefficients of obtained from the studied compounds, show that $GaAs_{0.5}Bi_{0.5}$ has the highest value at 40.2, followed by GaBi (37.0), GaAs (36.6), $GaAs_{0.75}Bi_{0.25}$ (31.2), and $GaAs_{0.25}Bi_{0.75}$ (30.4). These values were specifically observed in the ultraviolet (UV) region. Our results confirm the relationship between extinction and absorption coefficient as related by expression in Equation (11).

$$k(\omega) = \frac{\alpha}{4\pi} \quad (11)$$

Thus, materials with high extinction coefficients, such as GaAsBi alloys, are useful in optoelectronics, solar cells, infrared optics, and photodetectors due to their strong light absorption properties, enhancing device performance in applications like lasers, sensors, and photovoltaics [47].

Optical reflectivity

Optical reflectivity (R) is one of the most important properties for understanding the interaction of a material with photons. For the material, it relates to the refractive index (n) and extinction coefficient (k) as shown in Equation (12).

$$R(\omega) = \frac{(n-1)^2 + k^2}{(n+1)^2 + k^2} \quad (12)$$

All symbols have their usual meanings. The relationship of dielectric constant from optical reflectivity can be expressed as presented in Equation (13) [23];

$$R(\omega) = \left|\frac{\sqrt{\varepsilon(\omega)} - 1}{\sqrt{\varepsilon(\omega)} + 1}\right|^2 \quad (13)$$

Figure 6(g) shows the calculated optical reflectivity coefficient R(ω) for the studied compounds. R(ω) curve showed reflection values of: 0 eV: GaAs = 35.2%, $GaAs_{0.75}Bi_{0.25}$ = 43.1%, $GaAs_{0.50}Bi_{0.50}$ = 66.5%, $GaAs_{0.25}Bi_{0.75}$ = 52.2%, and GaBi = 47.8%. The highest reflectivity, Rmax = 73.1% was found in $GaAs_{0.50}Bi_{0.50}$ at 10.38 eV, while $GaAs_{0.25}Bi_{0.75}$ showed the lowest Rmax = 54.5% at 10.14 eV. This is due to the shrinking of the band gap which results in a sharp peak in UV region. This leads to increase in material conductivity as the absorption edge shifts to longer wavelengths as the band gap energy decreases. Moreover, these results give us an idea of the movement of free electrons from valence band (VB) to conduction band (CB) compared to the band structure [48]. The reflectivity values below 1 in the entire energy range suggest that the studied materials are good candidates for anti-reflection applications [49].

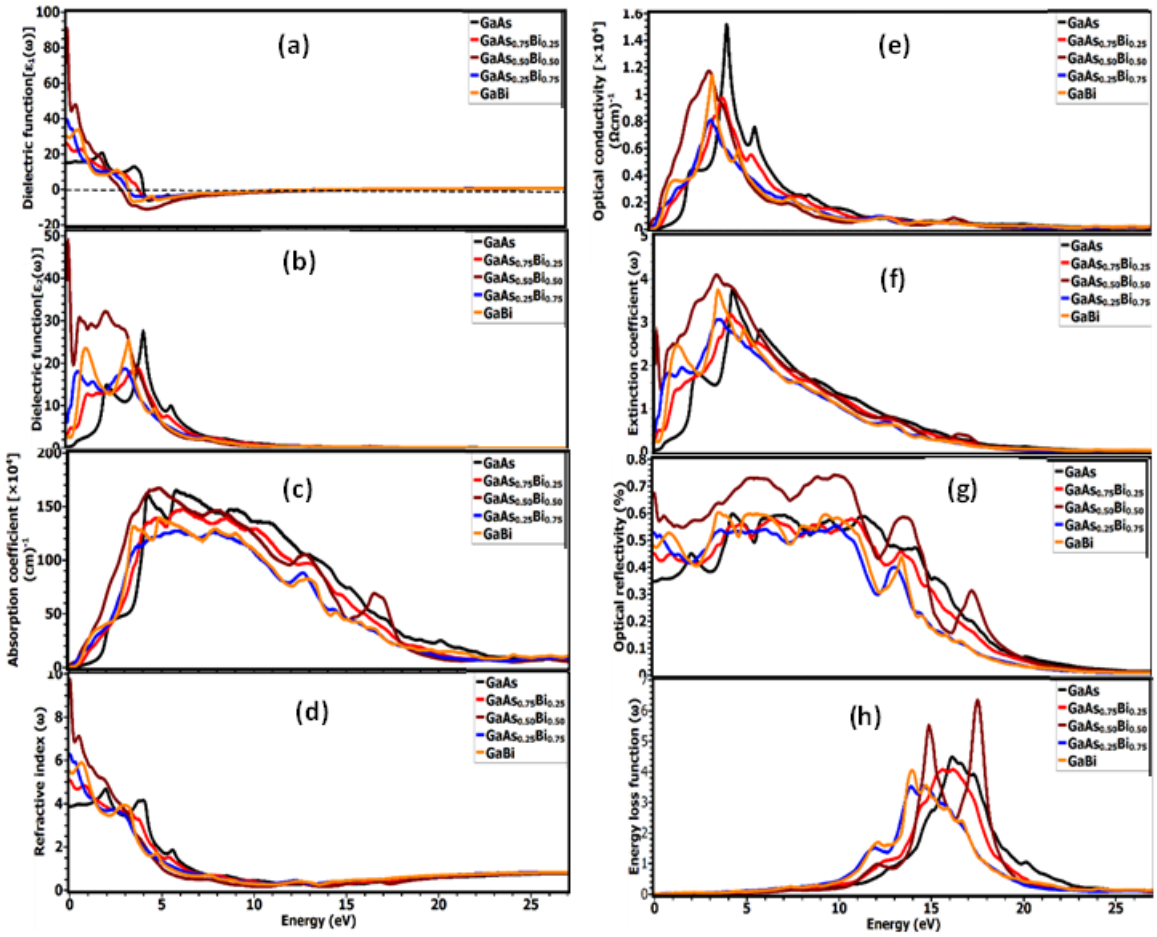

Figure 6: Calculated (a) real $\varepsilon_1(\omega)$, (b) imaginary $\varepsilon_2(\omega)$ of the dielectric function $\varepsilon(\omega)$, (c) absorption coefficient, (d) refractive index, (e) optical conductivity, (f) extinction coefficient, (g) optical reflectivity, and (h) energy loss function.

Energy loss function

Electron Energy Loss (EEL) is a valuable optical property measurement technique because it allows for the measurement of the entire energy range, including non-scattered and elastically scattered (zero-loss) electrons [50]. The energy loss function L(ω) is the energy dissipated as fast-moving electrons interact with electromagnetic fields while traversing through a material. Plasma oscillations are rapid fluctuations in electron density in conductive materials, such as charged fluids or metals, and occur in the UV region. By employing the dielectric constant expression, the energy loss function of the material can be derived from Equation (14).

$$L(\omega) = \frac{\varepsilon_2}{\left(\varepsilon_1{}^2(\omega) + \varepsilon_2{}^2(\omega)\right)} \quad (14)$$

The variation of the EEL function as a function of the energy is presented in Figure 6(b).

Low energy loss in the visible region means it can transmit light with minimal absorption or scattering, resulting in high optical performance in the visible spectrum. However, high energy loss in the UV region indicates strong absorption of UV light, which is beneficial for UV protection but detrimental for applications that require high transparency or optimal photonic performance.

Conclusion

This study uses DFT calculations within the FP-LAPW framework in WIEN2K to investigate the geometrical, electronic, and optical properties of

GaAs and GaAsBi alloys, using PBE-GGA and TB-mBJ to improve the band gap. The computed TDOS and PDOS for $GaAs_{1-x}Bi_x$ compounds using TB-mBJ show the band gap between VBM and CBM; As-4p primarily contributes to the conduction band while Ga-4s is dominating the valence band. The band gap variation with Bi doping demonstrates that PBE-GGA predicts metal (except GaAs) and TB-mBJ predicts direct band gap at Γ point, with significant band gap bowing due to Bi-induced structural relaxation and charge exchange, consistent with experimental data. $GaAs_{0.50}Bi_{0.50}$ has the highest static real dielectric constant (90.8) and imaginary dielectric constant (31.7 at 2.2 eV in the visible region), while other compounds have peak imaginary dielectric value in the ultraviolet region, indicating strong absorption due to interband transitions. Optical conductivity peaks in the ultraviolet region suggest high absorbance and free carrier generation, leading to net forward current, GaAs has the highest carrier mobility and conduction efficiency. Reflectivity shows $GaAs_{0.50}Bi_{0.50}$ has the highest R_{max} (73.1% at 10.38 eV), while $GaAs_{0.25}Bi_{0.75}$ has the lowest (54.5% at 10.14 eV) due to band gap shrinking, shifting the absorption edge to longer wavelengths and increases conductivity.

Acknowledgments

The authors would like to acknowledge financial support from the Tertiary Education Trust Fund Overseas Scholarship Award (TETFUND/ES/TSAS/MOU/FARA/2024/VOL.1) and computational resources from the Computational Materials Laboratory, Department of Pure and Applied Science, Ladoke Akintola University of Technology, Ogbomoso, Nigeria.

Conflict of Interest

No conflict of interest was declared by the authors in this work.

ORCID

A. A. Adewale: 0000-0001-8768-3876
C. De Conti: 0000-0002-3024-2671
S. O. Azeez: 0000-0001-5737-1388
K. O. Suleman: 0000-0002-9103-1974
H. O. Oyeshola: 0000-0002-1628-1455
A. J. Abiodun: 0000-0002-6596-2505
L. A. Sunmonu: 0000-0002-4305-8363

Reference

[1] T. Ishiyama, K. Nozawa, T. Nishida, T. Suemasu, K. Toko, Bayesian optimization-driven enhancement of the thermoelectric properties of polycrystalline III-V semiconductor thin films. *NPG Asia Materials*, **2024**, *16*, 17. [Google Scholar], [Publisher]

[2] J. Ai, M. Qin, M. Xue, C. Cao, J. Zhang, A.V. Kuklin, H. Wang, H. Zhang, Q. Zhang, H. Ågren, Recent advances of photodetection technology based on main group III–V semiconductors. *Advanced Functional Materials*, **2024**, *34*, 2408858. [Crossref], [Google Scholar], [Publisher]

[3] M.D. Mamo, Y. Zigyalew, S.E. Gelan, B. Ntsendwana, L. Sikhwivhilu, Advancements in NIR sensing for tuberculosis detection using dilute III-V semiconductors: current status and future prospects. *Frontiers in Sensors*, **2025**, *5*, 1521727. [Crossref], [Google Scholar], [Publisher]

[4] M.E. Twigg, S. Tomasulo, M.A. Stevens, N.A. Mahadik, N.A. Kotulak, M.K. Yakes, The Thermodynamics and Kinetics of Phase Separation in III-V Semiconductor Alloys. *Thin Solid Films*, **2024**, *793*, 140255. [Crossref], [Google Scholar], [Publisher]

[5] C.-Z. Zhao, Y. Guo, T. Wei, S.-S. Wang, J. Wang, Band gap energy of GaBixAs1-x in the As-rich range calculated by the First-principle calculation and the modified BAC model. *Applied Physics A*, **2021**, *127*, 605. [Google Scholar], [Publisher]

[6] A. Reshak, Bismuth-containing semiconductors GaAs1− xBix for energy conversion: Thermoelectric properties. *Materials Science in Semiconductor Processing*, **2022**, *148*, 106850. [Crossref], [Google Scholar], [Publisher]

[7] T. Paulauskas, V. Pačebutas, R. Butkutė, B. Čechavičius, A. Naujokaitis, M. Kamarauskas, M. Skapas, J. Devenson, M. Čaplovičová, V. Vretenár, Atomic-resolution EDX, HAADF, and EELS study of GaAs 1-x Bi x alloys. *Nanoscale Research*

Letters, **2020**, *15*, 121. [Google Scholar], [Publisher]
[8] V. Virkkala, V. Havu, F. Tuomisto, M.J. Puska, Modeling Bi-induced changes in the electronic structure of GaAs 1− x Bi x alloys. *Physical Review B—Condensed Matter and Materials Physics*, **2013**, *88*, 235201. [Google Scholar], [Publisher]
[9] Y. Zhang, A. Mascarenhas, L.-W. Wang, Similar and dissimilar aspects of III-V semiconductors containing Bi versus N. *Physical Review B—Condensed Matter and Materials Physics*, **2005**, *71*, 155201. [Google Scholar], [Publisher]
[10] P. Blaha, K. Schwarz, G.K. Madsen, D. Kvasnicka, J. Luitz, wien2k. *An augmented plane wave+ local orbitals program for calculating crystal properties*, **2001**, *60*, 155–169. [Google Scholar], [Publisher]
[11] JJ.P. Perdew, K. Burke, M. Ernzerhof, generalized gradient approximation made simple. *Physical review letters*, **1996**, *77*, 3865. [Google Scholar], [Publisher]
[12] P. Hohenberg, W. Kohn, Density functional theory (DFT). *Physical review letters*, **1964**, *136*, B864. [Crossref], [Google Scholar], [Publisher]
[13] G. Lehmann, M. Taut, On the numerical calculation of the density of states and related properties. *physica status solidi (b)*, **1972**, *54*, 469–477. [Crossref], [Google Scholar], [Publisher]
[14] Y. Wang, P. Wisesa, A. Balasubramanian, S. Dwaraknath, T. Mueller, Rapid generation of optimal generalized Monkhorst-Pack grids. *Computational Materials Science*, **2021**, 187, 110100. [Crossref], [Google Scholar], [Publisher]
[15] W. Yahya, A. Yahaya, A. Adewale, A. Sholagberu, N. Olasunkanmi, A DFT study of optoelectronic, elastic and thermo-electric properties of the double perovskites Rb2SeX6 (X= Br, Cl). *Journal of the Nigerian Society of Physical Sciences*, **2023**, 1418–1418. [Google Scholar], [Publisher]
[16] A. Kumar, H. Gupta, A. Kumar, A. Kumar, S.K. Sharma, B. Lal, N. Iram, Optoelectronic properties of Sb doped GaAs: DFT investigation. *Indian Journal of Physics*,**2024**, 1-10. [Crossref], [Google Scholar], [Publisher]
[17] K. Momma, F. Izumi, VESTA 3 for three-dimensional visualization of crystal, volumetric and morphology data. *Applied Crystallography*, **2011**, *44*, 1272–1276. [Crossref], [Google Scholar], [Publisher]
[18] F.E.H. Hassan, A. Postnikov, O. Pagès, Structural, electronic, optical and thermal properties of AlxGa1− xAsySb1− y quaternary alloys: First-principles study. *Journal of alloys and compounds*, **2010**, *504*, 559–565. [Crossref], [Google Scholar], [Publisher]
[19] A.A. Adewale, A. Chik, T. Adam, O.K. Yusuff, S.A. Ayinde, Y.K. Sanusi, First principles calculations of structural, electronic, mechanical and thermoelectric properties of cubic ATiO3 (A= Be, Mg, Ca, Sr and Ba) perovskite oxide. *Computational Condensed Matter*, **2021**, *28*, e00562. [Crossref], [Google Scholar], [Publisher]
[20] A.H. Reshak, H. Kamarudin, S. Auluck, I. Kityk, Bismuth in gallium arsenide: Structural and electronic properties of GaAs1− xBix alloys. *Journal of Solid State Chemistry*, **2012**, *186*, 47–53. [Crossref], [Google Scholar], [Publisher]
[21] M.H. Hachemi, M. Benchehima, K. Bencherif, H. Abid, The effect of N-incorporation on the structural and optoelectronic properties of GaP and GaAs for optical telecommunication applications: first-principles study. *Optik*, **2022**, *262*, 169282. [Crossref], [Google Scholar], [Publisher]
[22] D. Madouri, A. Boukra, A. Zaoui, M. Ferhat, Bismuth alloying in GaAs: A first-principles study. *Computational Materials Science*, **2008**, *43*, 818–822. [Crossref], [Google Scholar], [Publisher]
[23] A.A. Adewale, A. A. Yahaya, L.O. Agbolade, O.K. Yusuff, S.O. Azeez, K.K. Babalola, K.O. Suleman, Y.K. Sanusi, A. Chik, Optoelectronic and mechanical properties of gallium arsenide alloys: Based on density functional theory. *Chemical Physics Impact*, **2024**, *8*, 100594. [Crossref], [Google Scholar], [Publisher]
[24] H. Achour, S. Louhibi, B. Amrani, A. Tebboune, N. Sekkal, Structural and electronic properties of GaAsBi. *Superlattices and Microstructures*, **2008**, *44*, 223-229. [Crossref], [Google Scholar], [Publisher]
[25] M. Khelil, A. Abdiche, A. Ammari, B. Abbar, M. Guemou, R. Moussa, Bismides ternary alloys GaSb1− x Bi x: Structural, optoelectronic, and thermodynamic properties under pressure. *Journal of Materials Research*, **2022**, *37*, 1877–1891. [Google Scholar], [Publisher]

[26] Y. Cao, P. Zhu, J. Zhu, Y. Liu, First-principles study of NiAl alloyed with Co. *Computational Materials Science*, **2016**, *111*, 34–40. [Crossref], [Google Scholar], [Publisher]
[27] Y. Cao, C. Zhang, S. Zhou, Y. Xu, B. Peng, Z. Jiao, K. Luo, C. Tian, First-principles study of stability, electronic properties and anisotropic elasticity of Al3M (M= Ti, Ta, V, Nb, Hf) intermetallic compounds. *Physica B: Condensed Matter*, **2020**, *594*, 412294. [Crossref], [Google Scholar], [Publisher]
[28] H.P.R. Frederikse, R.F. Blunt, Photoeffects in intermetallic compounds. *Proceedings of the IRE*, **1955**, *43*, 1828-1835. [Crossref], [Google Scholar], [Publisher]
[29] A. Janotti, S.-H. Wei, S. Zhang, Theoretical study of the effects of isovalent coalloying of Bi and N in GaAs. *Physical Review B*, **2002**, *65*, 115203. [Google Scholar], [Publisher]
[30] O. Madelung, Semiconductors—basic data, *Springer Science & Business Media,* **2012**. [Google Scholar], [Publisher]
[31] M.I. Ziane, Z. Bensaad, T. Ouahrani, B. Labdelli, H.B. Nacer, H. Abid, First-principles prediction of the structural and electronic properties of zinc blende GaNxAs1− x alloys. *Materials science in semiconductor processing*, **2013**, *16*, 1138–1147. [Crossref], [Google Scholar], [Publisher]
[32] S.R. Tunio, S. Munir, M. Ayaz, F. Ahmad, An overview of corrosion types, corrosion testing and strategies to inhibit corrosion, *Journal of Engineering and Industrial Research,* **2024**, 5, 4, 204-227. [Crossref], [Google Scholar], [Publisher]
[33] P. Dang, Epitaxial Spin-Orbit and Magnetic Materials for Integration onto a Semiconductor Platform, *Cornell University*, **2021**. [Google Scholar], [Publisher]
[34] L. Bellaiche, S.-H. Wei, A. Zunger, Localization and percolation in semiconductor alloys: GaAsN vs GaAsP. *Physical Review B*, **1996**, *54*, 17568. [Crossref], [Google Scholar], [Publisher]
[35] S. Sakai, Y. Ueta, Y. Terauchi, Band gap energy and band lineup of III-V alloy semiconductors incorporating nitrogen and boron. *Japanese Journal of Applied Physics*, **1993**, *32*, 4413. [Google Scholar], [Publisher]
[36] M.S. Othman, E.B. Elkenany, Structural and optical properties of GaAs and InAs for doping Sb under the effect of pressure and temperature: DFT and EPM investigations. *Optical and Quantum Electronics*, **2022**, *54*, 807. [Google Scholar], [Publisher]
[37] A.A. Adewale, A. Chik, T. Adam, T.M. Joshua, M.O. Durowoju, Optoelectronic behavior of ZnS compound and its alloy: A first principle approach. *Materials Today Communications*, **2021**, *27*, 102077. [Crossref], [Google Scholar], [Publisher]
[38] L. Agbolade, A. Dafhalla, D. Zayan, T. Adam, A. Chik, A. Adewale, S. Gopinath, U. Hashim, A DFT study of the optoelectronic properties of B and Be-doped Graphene. *Journal of the Nigerian Society of Physical Sciences*, **2024**, 1730–1730. [Crossref], [Google Scholar], [Publisher]
[39] A. Soussi, L. Boulkaddat, A. Asbayou, N. Labchir, A. Elfanaoui, R. Markazi, K. Bouabid, A. Ihlal, A. Taleb, Structural, optical and electronic properties of La-doped ZnO thin films: experimental study and DFT calculations. *Physica B: Condensed Matter*, **2022**, *643*, 414181. [Crossref], [Google Scholar], [Publisher]
[40] I.A. Vovk, V.V. Lobanov, A.P. Litvin, M.Y. Leonov, A.V Fedorov, I.D. Rukhlenko, Band structure and intersubband transitions of three-layer semiconductor nanoplatelets, *Nanomaterials*, **2020,** *10*, 933. [Google Scholar], [Publisher]
[41] J.C. Martinez Anton, A.G. Manzanares, A.A. Fernandez-Balbuena, D.V. Molini, Measuring the absorption coefficient of optical materials with arbitrary shape or distribution within an integrating sphere, *Optics Express*, **2021**, *29*, 26287-26303. [Crossref], [Google Scholar], [Publisher]
[42] A. Kumar, M. Kumar, R. Singh, Magnetic, opto-electronic, and thermodynamic properties of half-metallic double perovskite oxide, Ba2YbTaO6: a density functional theory study. *Journal of Materials Science: Materials in Electronics*, **2021**, *32*, 12951–12965.-[Google Scholar], [Publisher]
[43] E.J. Beard, G. Sivaraman, Á. Vázquez-Mayagoitia, V. Vishwanath, J.M. Cole, Comparative dataset of experimental and computational attributes of UV/vis absorption spectra. *Scientific data*, **2019**, *6*, 307. [Google Scholar], [Publisher]
[44] H.J. Lee, M.M.A. Gamel, P.J. Ker, M.Z. Jamaludin, Y.H. Wong, J.P. David, Absorption

coefficient of bulk III-V semiconductor materials: A review on methods, properties and future prospects, *Journal of Electronic Materials*, **2022**, *51*, 6082–6107. [Google Scholar], [Publisher]
[45] M.A. Lahiji, A.A. Ziabari, First–principle calculation of the elastic, band structure, electronic states, and optical properties of Cu–doped ZnS nanolayers, *Physica B: Condensed Matter*, **2016**, *501*, 146–152. [Crossref], [Google Scholar], [Publisher]
[46] M.J.I. Khan, Z. Kanwal, Investigation of optical properties of CdS for various Na concentrations for nonlinear optical applications (A DFT study). *Optik*, **2019**, *193*, 162985. [Crossref], [Google Scholar], [Publisher]
[47] T. Smołka, M. Rygała, J. Hilska, J. Puustinen, E. Koivusalo, M. Guina, M. Motyka, Influence of the bismuth content on the optical properties and photoluminescence decay time in GaSbBi films. *ACS omega*, **2023**, *8*, 36355–36360. [Crossref], [Google Scholar], [Publisher]
[48] X. Zhang, M. Guo, W. Li, C. Liu, First-principles study of electronic and optical properties in wurtzite Zn1– XCdXO. *Journal of Applied Physics*, **2008**, *103*. [Crossref], [Google Scholar], [Publisher]
[49] M.J.I. Khan, Z. Kanwal, M.N. Usmani, M. Zeeshan, M. Yousaf, An insight into optical properties of Pb: CdS system (a theoretical study). *Materials Research Express*, **2019**, *6*, 065904. [Google Scholar], [Publisher]
[50] A. Laref, A. Altujar, S. Laref, S. Luo, Quantum confinement effect on the electronic and optical features of InGaN-based solar cells with InGaN/GaN superlattices as the absorption layers, *Solar Energy*, **2017**, *142*, 231–242. [Crossref], [Google Scholar], [Publisher]

Copyright © 2025 by authors and SPC (Sami Publishing Company) + is an open access article distributed under the Creative Commons Attribution License(CC BY), which permits unrestricted use, distribution, and reproduction in any medium, provided the original work is properly cited.